Original paper

THREE-DIMENSIONAL SHEAR-WAVE QUALITY FACTOR, QS(F), MODEL FOR SOUTH-CENTRAL GULF OF CALIFORNIA, MEXICO OBTAINED FROM INVERSION OF BROADBAND DATA

Sanjay Kumar[1]*, Anand Joshi[1], Raul R. Castro[2], Shri K. Singh[3], Sandeep Singh[1]

Received: May 8, 2020; accepted: December 2, 2020; published online: April 1, 2021.

RESUMEN

Se aplicó un esquema de inversión iterativo, inicialmente desarrollado por Hashida y Shimazaki (1984) y posteriormente modificado por Joshi *et al.*, (2010), para estimar el factor de calidad de onda corta tridimensional, *Qs (f)*, del centro-sur del Golfo de California, México. Es un área de 230 x 288 km que se divide en 108 bloques rectangulares de diferentes *Qs (f)*. Se utilizó 25 terremotos bien ubicados registrados en tres estaciones de banda ancha de la red regional RESBAN operada por CICESE (Centro de Investigación Científica y de Educación Superior de Ensenada, Baja California) y tres Sismógrafos de Fondo Oceánico (OBS, por sus siglas en inglés) de un conjunto del Experimento del Fondo Oceánico del Mar de Cortés (SCOOBA, por sus siglas en inglés). Este conjunto de datos permitió obtener estimaciones de *Qs (f)* de diferentes bloques, utilizando el algoritmo de inversión modificado. El *Qs (f)* se obtuvo a varias frecuencias en el rango de 0,16 ~ 8,0 Hz. Se encontró que la estructura *Qs* estimada se correlaciona con los modelos geológicos y tectónicos de la región propuestos en estudios previos. Se obtuvo una relación regional dependiente de la frecuencia que utiliza todos los valores de 1944 del factor de calidad de la onda de corte a 18 frecuencias diferentes en todos los bloques y se puede aproximar mediante una función de la forma $Qs\ (f) = 20\ f^{1.2}$. Esta relación es típica en una región tectónicamente activa con alta atenuación de onda *S* y es similar a las relaciones de atenuación reportadas por otros autores para la región del Valle Imperial, California.

PALABRAS CLAVE: *Qs*, atenuación, Golfo de California, Mexico, inversión de onda corta.

ABSTRACT

We apply an iterative inversion scheme, initially developed by Hashida and Shimazaki (1984) and later modified by Joshi *et al.,* (2010), to estimate three - dimensional shear - wave quality factor, $Q_s(f)$, of south-central Gulf of California, Mexico. An area of 230 km x 288 km in this region is divided into 108 rectangular blocks of different $Q_s(f)$. We use 25 well-located earthquakes recorded at three broadband stations of the regional network RESBAN operated by CICESE (*Centro de Investigación Científica y de Educación Superior de Ensenada, Baja California*) and three Ocean

**Corresponding author: sanjay.geokuk@gmail.com; anandfes@iitr.ac.in*

[1] Department of Earth Sciences, Indian Institute of Technology Roorkee, Roorkee, Uttarakhand, India.

[2] Centro de Investigación Científica y de Educación Superior de Ensenada (CICESE), División Ciencias de la Tierra, Departamento de Sismología, Ensenada, Baja California, México.

[3] Instituto de Geofísica, UNAM, Ciudad Universitaria, México City, México.

Bottom Seismographs (OBS) of the Sea of Cortez Ocean Bottom Array (SCOOBA) experiment. This dataset permits us to obtain $Q_s(f)$ estimates of different blocks using the modified inversion algorithm. $Q_s(f)$ is obtained at various frequencies in 0.16 ~8.0 Hz range. We found that the estimated Q_s structure correlates with geological and tectonic models of the region proposed in previous studies. A regional frequency-dependent relation using all 1944 values of shear-wave quality factor is obtained at 18 different frequencies in all blocks can be approximated by a function of the form $Q_s(f) = 20\, f^{1.2}$. This relation is typical in a tectonically active region with high *S*-wave attenuation and is similar to attenuation relations reported by other authors for the Imperial Valley, California region.

KEY WORDS: Q_s, Attenuation, Gulf of California, Mexico, Shear-wave inversion.

INTRODUCTION

The Gulf of California (GoC) is obliquely rifted that connects the East Pacific rise spreading ridge in the south with the San Andreas Fault in California. The trans-tension between the North American and Pacific plates resulted in the generation of the large earthquakes in the GoC along with the transform faults and the spreading ridges (Castro *et al.,* 2011b; Castro *et al.,* 2017b). The earthquakes in this region follow a fairly linear trend along the southeastward direction from southern California to the southern end of the Gulf of California, Mexico. The transform faults are associated with right lateral strike slip faulting while normal faulting is observed near the spreading centres. The northern GoC comprises the complex transform fault geometry and is the major reason for large (Ms > 6) earthquakes in this region (Goff *et al*., 1987, Castro *et al.,* 2017b). The observed mechanism of faulting in this region is oblique -normal faulting in nature (Persaud *et al*., 2003, *Castro et al.,* 2017b). On the other hand, the southern GoC comprise the ridge transform fault system along with the hot zones under the weak crust is the dominant mode of rupturing to generate large (Mw: 7.0 (January 7, 1901)) earthquakes (Pacheco and Sykes, 1992). These factors along with the oblique plate motion also resulted in the rapid rupturing of southern region (Umhoefer 2012).

Seismic waves generated from an earthquake experienced the attenuation of wave amplitude at distant locations from the source. The attenuation rate of seismic wave amplitude is very sensitive to the presence of fluids in the rocks, temperature conditions, the composition of rocks and other factors, while propagating through the earth interior. Local geology or the site condition at a location also plays a key role during an earthquake by amplifying or attenuating the seismic waves at different sites. The seismic attenuation is described in terms of inverse of a dimensionless parameter known as the Quality factor (Knopoff 1964). In 1984, Hasida and Shimazaki introduced a technique to estimate the 3D Q-structure using the intensity data for Tohoku region, Japan. Later Satake and Hasida (1989) and Nakamura and Uetake (2002) has used this method to distinguish and understand the behaviour of low and high attenuation regions for north Island, New Zealand and Pacific sea plate, Japan. Besana *et al*., (1997) has studied the regional effects of subsurface structures like arcs, slabs and continental material using the 3D Q-structure for Philippine region. Later, Nakamura and Uetake (2002) and Joshi *et al.,* (2010) has modified the technique and use the acceleration data to obtain the attenuation structure for Tohoku, Japan and Uttarakhand, India regions. Attenuation studies around the world based on Q^{-1} values have been used to characterize the tectonic regions e.g. stable, volcanic, and seismically active (Joshi *et al.,* 2010; Castro *et al.,* 2008; Kumar *et al.,* 2015). The less attenuating media in a region is characterized by the high Q value and the vice versa.

Various attempts have been made to understand the attenuation behaviour of seismic waves in GoC and the surrounding region. For the southern region, Ortega and González (2007) has followed the general least square regression of strong motion data to determine the S or Lg wave attenuation for the

La Paz–Los Cabo region, Baja California, Mexico. The obtained results were further validated, using the coda normalization method and reported a lower attenuation for the La Paz–Los Cabo inland region. Later, Ortega and Quintanar (2011) used the offshore earthquake data and compared the propagation characteristics of S waves reported by Ortega and González (2007) with the P wave propagation characteristics following the same method. Vidales-Basurto *et al.,* (2014) has conducted the attenuation study in the south central GoC region to understand the tectonic structure of gulf region. The results obtained based on the different source receiver distance depicts the higher body wave attenuation along the oceanic spreading centres. Also, high attenuation is observed towards the southern gulf region compared to the central gulf region. Later, Rodríguez- Lozoya *et al.,* (2017) estimated the coda attenuation for central gulf region and observed a similar higher attenuation for the southern sub region. Also, Castro *et al.,* (2017b) determined the body wave attenuation and source functions for the gulf region using the foreshocks, aftershocks and the main shock (Mw= 6.6) of event occurred on October 19, 2013, along the Farallon fault region. For central gulf region, Quintanar *et al.,* (2019) have analysed the foreshocks, main shock (Mw=6.6) and aftershocks of January 4, 2006 San Pedro Martir earthquakes. They obtained the source parameters, fault geometry and fault slip distribution for the earthquake and later used them to study the attenuation behaviour of gulf region. More, recently Castro *et al.,* (2019) studied the one-dimensional variability of Q_S in the southern region of GoC at selected frequencies. They reported an increase of Q_S with increase of frequency but small variation of Q_S has been observed with depth (5-40 km) at individual frequencies.

The present article uses the approach given by Joshi *et al.,* (2010) to obtain three- dimensional attenuation structure in a broad frequency range. We use data from 25 earthquakes recorded both onshore and offshore by Ocean Bottom Seismographs (OBS) deployed in the study area of south-central Gulf of California (GoC) region. This tectonically complex region comprises a system of short spreading centres and transform faults and is considered as a high seismicity zone (Sumy *et al.,* 2013). The attenuation structure must have a strong correlation with the tectonic environment and the seismic wave velocity (Lizarralde *et al.,* 2007; Luccio *et al.,* 2014) and for this reason, is important to evaluate the attenuation characteristics of GoC.

TECTONIC STRUCTURE OF STUDY AREA

The Gulf of California (GoC) is relatively young, oblique rift system that formed with the cessation of the Farallon plate subduction under the North American plate about 12 million year ago (Lonsdale, 1989). The evolution of the GoC extensional province occurred in two stages; stage-I: extension and separation of the continents that resulting in the formation of marine basins; stage-II: is being continued till today is the expansion of seafloor and structure of transform faults (Stocks and Hodges 1989; Bennett *et al.*, 2007; Vidales-Basurto *et al.*, 2014). The GoC is comprised a group of stepping faults, seafloor spreading, ridges and the right lateral strike-slip transform faults which collectively form a continental rift system. Consequently, it facilitates the Pacific Plate to move apart from the North American plate. However, an anomalous left lateral strike slip faulting has been observed for September 1, 2007 main shock (Mw= 6.1) and its subsequent aftershocks activities in the southern gulf region (Ortega & Quintanar, 2010). The unusual characteristics of main shock and the high rate of aftershock (more than 800 during a period from September to December 2007) activities for a transform fault is believed to be a combination of narrow bathymetry, growing seafloor and stress interaction along the continental oceanic transition (COT) boundary. The major tectonic faults and the corresponding oceanic basins in GoC is shown in Fig 1. The crust underneath the ocean basins in GoC differs in terms of thickness, rifting style, sea floor spreading, and magmatism.

The south central GoC has a distinct rifting style compare to the surrounding region. Lizarralde *et al.*, (2007) has observed that evolution of rifting in this region is primarily controlled by the magmatic depletion of mantle. The anomalous Guaymas basin in the central region is considered as magmatic since the beginning of breakup (~ 6 m.a.) and possess the largest new igneous crust spread over ~280 km. The intrusive magmatism in the overlain sediments has resulted in the formation of sills over a large distance from the spreading centre (Aragón-Arreola *et al.*, 2005). On the other hand, the Farallon and Pescadero segment in the south of Guyamas basin have narrow ocean basins with nascent or no sea floor spreading (Lizarralde *et al.*, 2007).

Data Used

The highly active south-central GoC was monitored by regional seismic network of NARS- Baja (Network of Autonomously Recording Seismographs) and the Broadband Network (RESBAN) operated by the CICESE (Avila-Barrientos and Castro, 2016). The present study also used some of the events recorded offshore by eight Ocean bottom Seismographs (OBS's) deployed under the Sea of Cortez Ocean Bottom Array (SCOOBA) experiment in the Guaymas and Alarcon basins (Sumy *et al.,* 2013). This offshore network was operative only from October 2005 to October 2006. For the present study, 25 earthquakes recorded on both onshore and offshore stations deployed in the GoC were used. The offshore OBS's are equipped with four components (two horizontal, one vertical and one pressure component) to record the ground motion at the recording rate of 32.25 samples/s (Sumy *et al.,* 2013). The onshore broadband system, operated by CICESE, is equipped with three-component sensors, recording at 20 samples/s (Castro *et al.,* 2017b, 2018). The recording stations and the epicentral location of the earthquakes used in this study are shown in Fig. 1. The calculated hypocentral parameters of the selected earthquakes and the stations used are listed in Table 1.

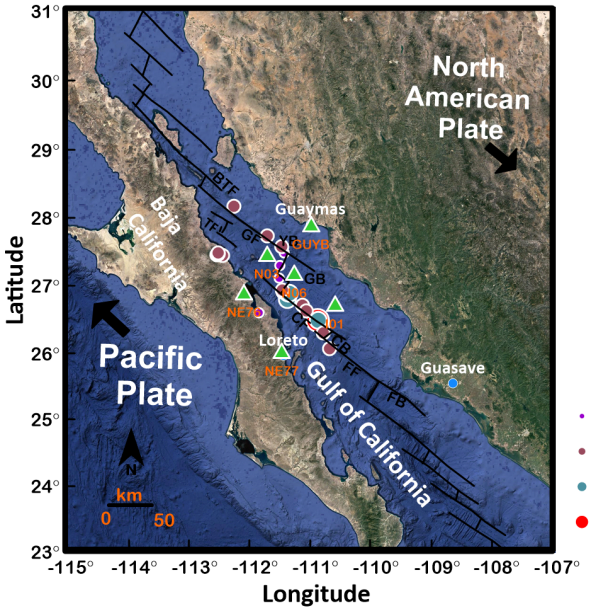

Figure 1. Map showing the location of recording stations (green triangles) and epicentres (circles) of the earthquakes selected. The purple, brown, sea green and the red circle are different magnitude bins and has been scaled as per the magnitude of earthquakes. The location of faults is taken from Aragon-Arreola *et al.,* (2005) and Dorsey *et al.,* (2013). DB= Delfin Basin, BTF= Canal de Ballenas Transform Fault, YB= Yaqui Basin, GF= Guaymas fault, GB= Guaymas Basin, CF= Carmen Fault, CB= Carmen Basin, FF= Farallon Fault, FB= Farallon basin, TF= *Tortuga Fault*. The black arrows represent the plate motion.

Fourier amplitude spectra of S-wave windows from 98 records have been used as an input in the inversion. The spectral input files consist of 18 discrete values of S-wave spectral amplitudes that range from 0.16 Hz to 7.94 Hz. Fig. 2 shows a sample of the amplitude spectra of a few stations along with the epicentral distance (ED). The earthquakes selected were relocated by Castro *et al.*, (2011) using

records from the regional stations of the NARS-Baja (Trampert *et al.,* 2013) and RESBAN (Castro *et al.,* 2018b) arrays. Some of the events were located by Sumy *et al.*, (2013) using OBS's. Fig. 3 represents the magnitude hypocentral distance plot for selected events. The records were corrected for instrument response and they were baseline corrected. The S-wave windows length used to calculate the fourier amplitudes amplitudes varies between 2 s for local hypecentral distance to 75 s for regional distance. The time window starts a few seconds before the first *S*-wave arrival and ends before the surface waves arrive. The spectral records were smoothed choosing 20 equidistant frequencies, between 0.16 and 7.94 Hz, on a logarithmic scale and averaging the amplitudes using a variable frequency band of ± 25% over the central frequencies chosen (Castro *et al.,* 2017a).

The site response functions determined by Vidales-Basurto *et al.,* (2014) and Avila-Barrientos and Castro (2016) for both the NARS-Baja and the RESBAN broadband stations were used to correct the spectral amplitudes for site effects.

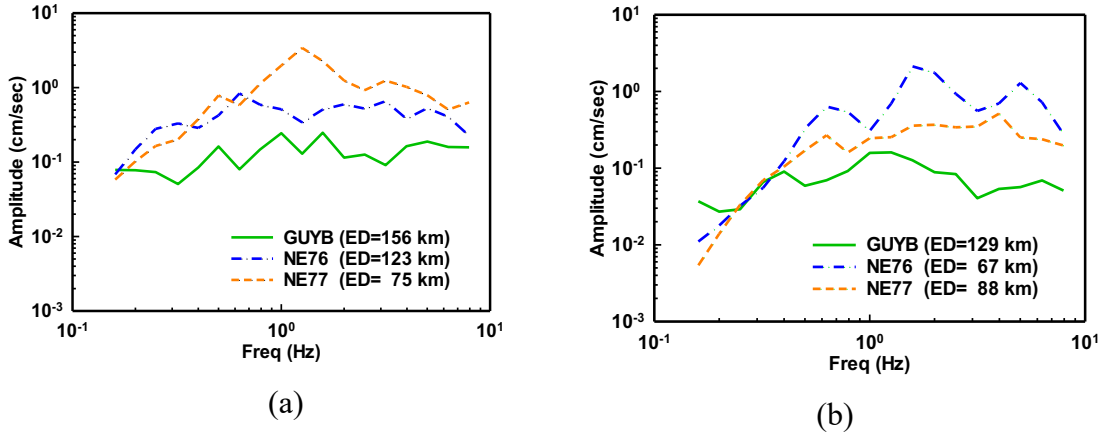

Figure 2. Amplitude spectra of S-phase recorded at stations GUYB, NE76 and NE77 from the following earthquakes: (a) 12/03/2003 (M_w=6.3) (b) 30/07/2006 (M_w=5.9)

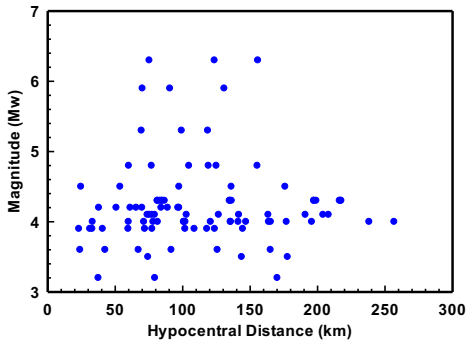

Figure 3. Spatial distribution of magnitude versus hypocentral distance of analyzed earthquakes. The selected earthquakes have Mw ranging from 3.2 to 6.3 with hypocentral distance from 20 km to 260 km.

A rectangular block of dimension 230 km to 288 km was selected on the basis of coverage area of seismic network and availability of events within it. This block is divided into six sub-blocks with individual sub-block having a rectangular area 38 km x 48 km. These blocks are further extended by three blocks of thickness upto a depth of 12 km; thereby dividing entire area into individual three dimensional blocks of size 38 km x 48 km x 4 km. The location of the rectangular block is shown in Fig. 4 along with the structural features of the study region. Inset zoom in the Fig. 4 represents the straight-line ray path projection in sub blocks between the events and the recording stations. The spectral amplitudes shown in Fig. 2 are from earthquake located between the first and third row of considered rectangular block.

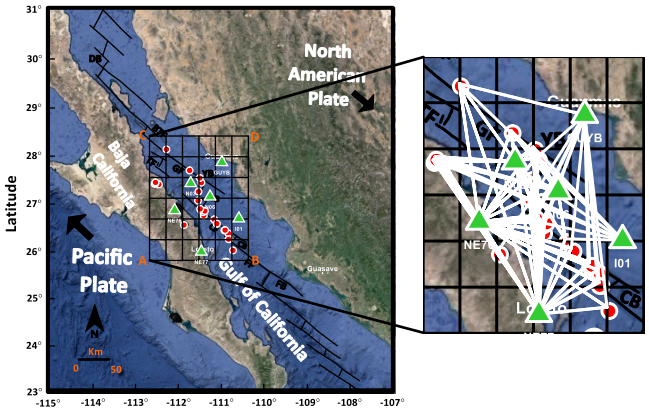

Figure 4. Map with location of the study area and the rectangular grid (ABCD) of the volume sampled, along with the tectonic features in the rectangular grid (ABCD). Red circles with white boundary indicate the epicentres of selected earthquakes. Inset zoom shows the projection of ray paths between the selected events and the recording stations in the studied area.

Table 1. Parameters of earthquake used in the present work.

S. No.	Year	Month	Day	Hour	Minute	Second	Latitude°	Longitude°	Depth (km)	Magnitude (Mw)	Recording Stations
1	2002	12	6	6	24	12.256	26.3152	-110.7364	8.6	4.0	GUYB, NE76, NE77
2	2002	12	7	1	33	45.285	26.0794	-110.633	9.8	4.1	GUYB, NE76, NE77
3	2002	12	8	17	45	17.391	26.3141	-110.7159	16.2	3.5	GUYB, NE76, NE77
4	2003	1	19	16	46	30.147	26.9204	-111.3973	2.0	4.0	GUYB, NE76, NE77
5	2003	3	12	23	41	30.561	26.4994	-110.8355	2.0	6.3	GUYB, NE76, NE77
6	2003	3	13	4	23	7.463	26.4337	-110.7387	8.3	4.0	GUYB, NE76, NE77
7	2003	3	13	14	38	20.61	26.6403	-111.0145	15.6	4.1	GUYB, NE76, NE77
8	2003	3	22	17	55	41.519	26.5048	-110.8193	5.3	4.8	GUYB, NE76, NE77
9	2004	2	18	19	30	39.033	26.6345	-111.0169	7.2	3.9	NE76, NE77
10	2004	8	7	10	41	24.442	26.6103	-111.7947	6.2	3.2	GUYB, NE76, NE77
11	2006	4	20	3	40	41.28	28.194	-112.21	3.0	4.0	GUYB, I01, N03, NE76, NE77
12	2006	4	23	7	50	40.05	27.498	-111.38	4.0	3.6	GUYB, I01, N03, N06, NE76, NE77
13	2006	5	11	5	58	18.04	27.311	-111.45	1.0	3.9	I01, N03, N06, NE76, NE77
14	2006	5	28	14	0	56.78	26.948	-111.41	12.0	4.8	GUYB, NE76, NE77
15	2006	5	28	14	18	2.23	26.904	-111.3	4.0	5.3	GUYB, NE76, NE77
16	2006	6	11	4	11	36.33	26.726	-111.08	5.0	4.2	I01, N03, N06, NE77
17	2006	6	16	8	46	44.74	27.595	-111.42	2.0	4.5	I01, N03, N06, NE76, NE77
18	2006	7	30	1	20	56.96	26.809	-111.326	19.4	5.9	GUYB, NE76, NE77
19	2006	8	7	2	50	53.05	27.503	-112.47	6.0	4.3	I01, N03, N06, NE76, NE77
20	2006	8	8	4	29	32.29	27.472	-112.49	5.0	4.3	I01, N03, N06, NE76, NE77
21	2006	8	8	21	36	35.8	27.461	-112.39	10.0	4.1	I01, N03, N06, NE76, NE77
22	2006	8	9	23	32	19.38	27.485	-112.47	5.0	4.3	I01, N03, N06, NE76, NE77
23	2006	8	11	17	55	11.5	26.881	-111.34	5.0	4.2	I01, N03, N06, NE76, NE77
24	2006	9	12	18	56	28.36	27.753	-111.66	2.0	4.0	I01, N03, N06, NE76, NE77
25	2006	9	25	13	4	5.65	27.122	-111.46	5.0	3.9	I01, N03, N06, NE76, NE77

METHODOLOGY

The inversion procedure used is based on the method proposed by Aki and Lee (1976). A cartesian co-ordinate system has been used to represent the distribution of the shear wave attenuation coefficient of the study region. The region was divided into 108 rectangular blocks with each block having a different $Q_s(f)$ value. The corners of these rectangular blocks on the surface of the Earth are assumed as the observation points. For an earth model having several blocks with different shear wave attenuation coefficient values, $Q_s(f)$ for a given frequency f, the spectral acceleration A(f) can be given by the following relation (Hashida and Shimazaki 1984):

$$A(f) = S(f).G.g_a.\exp \sum_r (C_{pqr}.T_{ijr}) \quad \text{..... (1)}$$

$$G = \frac{1}{R}$$

$$C_{pqr} = -\pi f/Q_{pqr}(f)$$

Where S(f) denotes the source acceleration at frequency f, G represents the geometrical spreading function and R the hypocentral distance, g_a is site amplification term and T_{ijr} represents the travel time of the ray in rth block having attenuation coefficient C_{pqr}. The parameter $Q_r(f)$ represents the frequency dependent quality factor in the rth rectangular block. The subscript i, j represents the ith station and the jth event, respectively. To solve equation (1), an initial three dimensional $Q_{pqr,o}(f)$ model of earth is assumed. The subscripts p, q is used to define the blocks along the two-horizontal directions of the rectangular area as shown in Fig. 5. The subscript r identifies the rectangular blocks in the downward direction. The initial input model is based on the velocity and Qs models (Rebollar *et al.,* 2001 and Paulseen and de Vos (2017)) available for the studied region. The initial guess of source strength $S^{cal}(f)$ for inversion has been calculated using initially assumed Q model and recorded spectral acceleration in the following relation:

$$S_{ij}^{cal}(f) = \frac{A_{pq}^{inter}(f)}{G.g_a.\exp \sum_r (C_{pqr,o}.T_{ijr})} \quad \text{..... (2)}$$

Where $S_{ij}^{cal}(f)$ defines the calculated source strength at frequency f, $A_{pq}^{inter}(f)$ is spectral acceleration obtained after interpolation at each observation points at frequency f and $C_{pqr,o}$ is initially assumed attenuation in rth block. This value of spectral acceleration is calculated from the earthquake records. Because it is nearly impossible to have a network in which the observation points are placed at each corner of the grid at equal spacing, we are required to calculate contours of spectral acceleration in the considered rectangular area. The amplitude spectrum of S-phase of a particular earthquake, recorded at different station is used to prepare the spectral acceleration contours at frequency, f, using kriging interpolation. The spectral acceleration $A_{pq}^{inter}(f)$ values obtained at different observation points from the contours has been used in the equation (2) to obtain the initial source strength $S_{ij}^{cal}(f)$ at frequency f. In the present study the input data used for inversion has been corrected for site effects, therefore the site amplification factor g_a is fixed to one. The average value of source strength $S_{ij}^{cal}(f)$ calculated at different frequencies is further used to calculate the spectral acceleration $A_{ij}^{cal}(f)$ using equation (1).

If the observed spectral acceleration at any point is defined as $A_{ij}^{obs}(f)$, then the relation between

$A_{ij}^{obs}(f)$, the actual attenuation coefficient C_{pqr} and source strength $S_o(f)$ can be calculated using same equation (1). By dividing observed $A_{ij}^{obs}(f)$ and calculated $A_{ij}^{cal}(f)$ spectral acceleration, following equation is obtained:

$$A_{ij}^{obs}(f)/A_{ij}^{cal}(f) = (S_o(f)/S^{cal}(f)).\exp \sum_r(C_{pqr,o} - C_{pqr}).T_{ijr) } \text{ …….. (3)}$$

Natural logarithms on both the sides of above equation gives the following equation:

$$\ln (A_{ij}^{obs}(f)/A_{ij}^{cal}(f)) = \ln ((S_o(f)/S^{cal}(f))) + \sum_r(\delta C_{pqr}).T_{ijr}) + e \text{ ……. (4)}$$

Where $\delta C_{pqr} = C_{pqr,o} - C_{pqr}$

$$Res_{ij}(f) = \ln (A_{ij}^{obs}(f)/A_{ij}^{cal}(f))$$

"$Res_{ij}(f)$" represents the residual acceleration and is used as a known variable for the inversion process. The term e stands for error in calculation.

The parameters δC_{pqr} and T_{ijr} on the right-hand side of equation (4) can be calculated from the initial velocity model using ray theory. For a particular earthquake, the total number of equations corresponds to the number of observation points. In equation (4), $A_{ij}^{obs}(f)$ and $A_{ij}^{cal}(f)$ represents the observed and calculated spectral acceleration, and $S_o(f)$ and $S^{cal}(f)$ are observed and calculated source strength, respectively. Equation (4) is inverted to get C_{pqr} in each block and the ratio of observed and calculated source strength. In the inversion scheme, we incorporate a new iteration by substituting the value of source strength obtained from the first inversion.

The process of obtaining spectral acceleration at each point in the grid is obtained directly from an inbuilt subroutine that calculates contour values at different positions using the spectral data of S phase from each record analysed. Fourier amplitude spectra of 98 records has been used to obtain 18 three dimensional structures in the discrete frequency range from 0.16 Hz to 7.94 Hz.

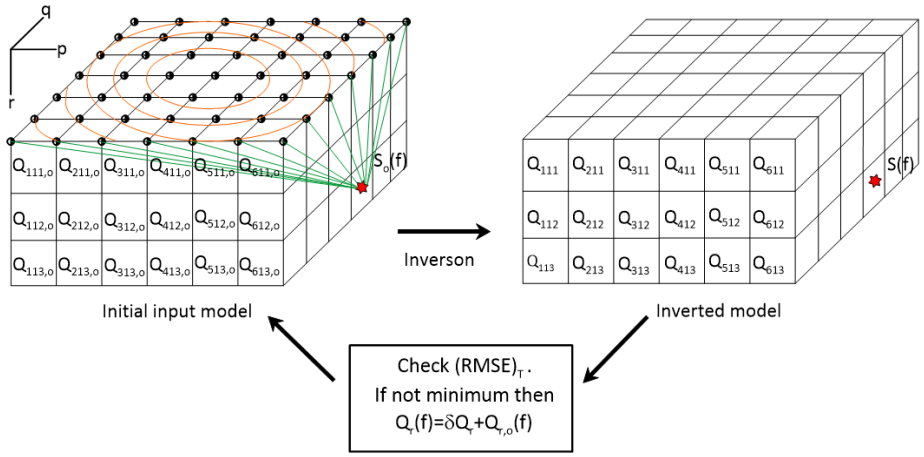

Figure 5. Schematic representation of inversion of initial $Q_{pqr,o}$ model used to obtain the final Q_{pqr} model for different rectangular blocks. The orange circles represent the spectral acceleration contours at frequency f and is used to obtain the calculated spectral acceleration $A_{ij}^{cal}(f)$. Red star and half black circles symbolize the theoretical position of earthquake and the observation points, respectively. Green lines depict the theoretical straight line ray path from source to the observation points through the different Q_{pqr} model blocks in time T_{ij}^{pqr}.

TESTS FOR INPUT PARAMETER

The results of the inversion depend on the quality of input data (e.g. Joshi 2007). In the present work, the input data consists of the initial velocity model, the initial shear wave attenuation model, hypocenters distances and distribution of the selected events and the S- wave window chosen to calculate the spectral acceleration values. To test the sensitivity of these parameters, various input parameter tests were performed, like the effect of the velocity model and the resolution of the final attenuation model on the input parameters.

Bakus and Gilbert (1968) have used the resolution matrix to check the suitability of model matrix, which can be defined for the damped least-square inversion using the following relation:

$$R = (G^T G + \lambda I)^{-1} G^T G \quad \ldots\ldots\ldots\ldots\ldots\ldots\ldots\ldots\ldots\ldots\ldots\ldots \quad (5)$$

Where R represents the resolution matrix and when R equals to the unit matrix, the obtained solution is unique. As the resolution matrix deviates from the unit matrix, the resolution becomes poorer. Several attempts had been made to check the resolution matrix for simple cases, and the obtained results are close to identity matrix for damped least-square inversion method. This simple case is also used for testing the reliability of the developed algorithm for inversion. For the actual case of acceleration data, the final model is selected based on the minimization of root mean square errors (RMSE). The $RMSE_A$ between the observed and calculated spectral acceleration at a particular frequency is given by the following equation:

$$\mathrm{RMSE_A} = \left[\frac{1}{N}\sum_{i=1}^{N}\left(A_i^{obs} - A_i^{cal}\right)^2\right]^{1/2} \quad \ldots\ldots\ldots\ldots\ldots\ldots \quad (6)$$

Where A_i^{cal} and A_i^{obs} denote the calculated and the observed spectral acceleration values at N number of observation points. The RMSE between the observed and calculated data and model matrix can also be computed using the equation (6). A reliable solution is obtained when all the errors are minimized simultaneously. The final model is selected based on the minimization of the following equation:

$$(\mathrm{RMSE})_T = (\mathrm{Nor(RMSE)_{dat}} + \mathrm{Nor(RMSE)_{mod}} + \mathrm{Nor(RMSE)_A})/3 \quad \ldots\ldots\ldots\ldots\ldots \quad (7)$$

Where $\mathrm{Nor(RMSE)_{dat}}$ and $\mathrm{Nor(RMSE)_{mod}}$ represents the normalized RMSE due to data and model matrix. However, it is hard to minimize $(\mathrm{RMSE})_{dat}$, $(\mathrm{RMSE})_A$ and $(\mathrm{RMSE})_{mod}$ simultaneously for the same iteration, that is $(\mathrm{RMSE})_T$ always differs from the ideal value equal of one. Moreover, the choice of the initial model and the number of input events also plays a vital role to obtain the final solution.

TEST FOR VELOCITY MODEL

Results of inversion depend upon the appropriate velocity models used for the parameterization of earth's structure as the properties mainly change with depth due to compaction, sedimentation and thermal changes. A numerical experiment was performed to check the distribution of shear wave velocity (*Vs*) model and quality factor (*Qs*) value for one layer, two layers and three layers model. The initial velocity model with different *Qs* values is shown in Table 2. The input models are based on the velocity and *Qs* models used by Rebollar *et al.,* (2001) and Paulseen and de Vos (2017) for the Gulf and Baja California region. The final model selection is based on the minimization of $(\mathrm{RMSE})_T$. In the present work, error reduces from 252 x 10^{-4} to 134 x 10^{-4} when

model changes from homogeneous to three layer model. Table 3 shows error estimates for homogeneous and layered earth models. Fig. 6 shows the dependency of the final attenuation structure on the initial velocity model and their corresponding error estimates. The three models predict a local high *Qs* zone but is located more accurately for two and the three-layer models. The 3-layer model provides more details of the *Qs* structure and fits the data better.

Table 2. Initial homogeneous layer, two layer and three layer earth models.

	Three layer model		Two layer model		One layer model	
Depth (km)	Velocity (km/s)	Qs	Velocity (km/s)	Qs	Velocity (km/s)	Qs
0-4	2.83	40	2.83	20	3.27	50
4-8	3.18	50	3.49	65	3.27	50
8-12	3.80	90	3.49	65	3.27	50

Table 3. Estimate of $(RMSE)_T$ and its iteration for homogeneous layer, two layer and three layer earth model.

Initial earth model	Minimum $(RMSE)_T$ (10^{-4})	Number of iterations corresponding to final model
Homogeneous layer	252	2
Two layer	179	3
Three layer	134	3

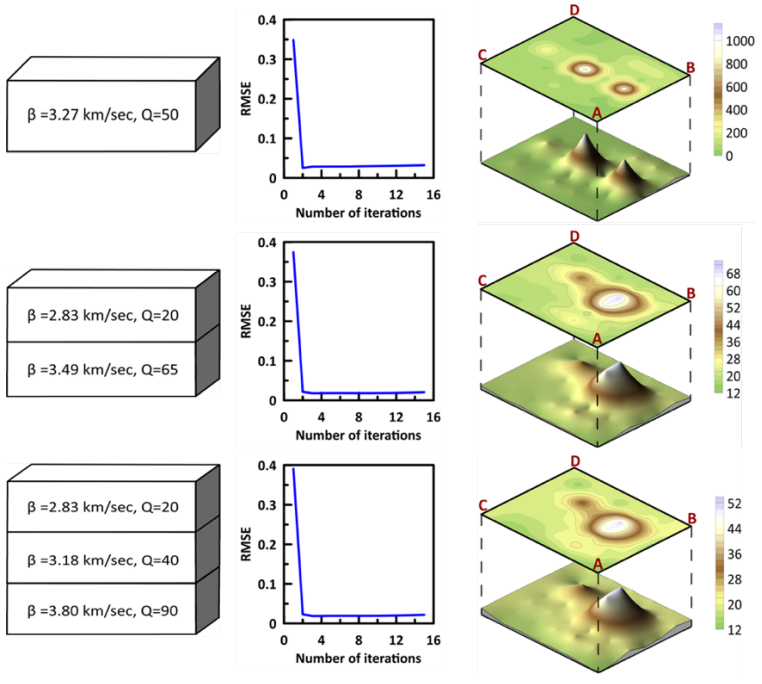

Figure. 6. Dependency of final attenuation structure on the initial velocity models with different Q values. (a) represents the initial layer model, (b) the error corresponding to input layer model and (c) the surface layer (0-4 km) attenuation structure contours along with the 3D projection of contour values at 1 Hz frequency.

TEST FOR INPUT DATASETS

In this experiment, the behaviour of the number of input earthquake data on final attenuation structure has been studied by removing some input earthquakes sequentially. The final attenuation model obtained using the data set of ten, fifteen and twenty-five earthquakes are shown in Fig. 7. This figure shows horizontal projections of the Q estimates obtained at different depths (0-4 km, 4-8 km and 8-12 km). Since the three data sets used for this test sample different crustal volumes, the resulting Q contours are significantly different. It is clear that the greater the number of sources used the better is the fit and the convergence. Table 4 shows error estimate and the number of iterations corresponding to the final solution for ten, fifteen and twenty-five earthquakes data sets, respectively. It is observed from the inversion that the $(RMSE)_T$ decreases with increase in input earthquake data and attenuation structure become much visible compared to that obtained using fewer earthquakes.

Table 4: Estimate of $(RMSE)_T$ and its iteration with the number of input earthquake data.

Input number of earthquakes	$(RMSE)_T$ (10^{-6})	Number of iterations
10	442	9
15	560	3
25	348	3

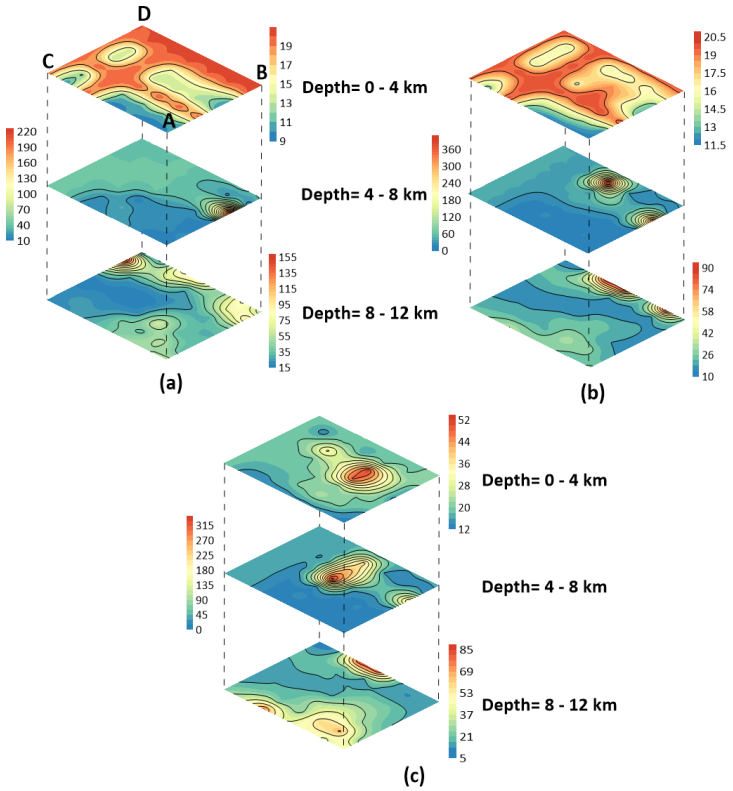

Figure 7. Dependency of the final attenuation model on the number of input earthquake data. Final models obtained for input data set of (a) Ten (b) Fifteen and (c) Twenty-Five earthquakes.

RESULTS AND DISCUSSION

The geologically young and tectonically complex region of the GoC provides an opportunity to understand the attenuation characteristics of the crust in this region. We have determined a three-dimensional (3-D) attenuation structures for the south - central GoC region. The area of interest has been divided into the 108, 3-D rectangular blocks of dimensions 38 km x 48 km x 4 km. The selection of dimensions of the rectangular blocks is based on the location of recording stations and earthquake epicentres. All stations and hypocenters of earthquakes lie within these rectangular blocks.

In the present article, the three - dimensional attenuation structure has been determined from a total of 1944 estimates of the shear- wave quality factor at 18 discrete frequencies. The resolution matrix of the inversion has significant importance in understanding how much information has been recovered in individual blocks. Fig. 8 is a 2-D view of the resolution matrix for the individual blocks. Blocks with resolution value > 0.7 have been considered as well resolved, and it has been observed that almost all the blocks in the region sampled are in general well resolved. Fig. 9 displays the source-station ray paths and illustrates the coverage of the volume sampled, which is good at depths above 10 km.

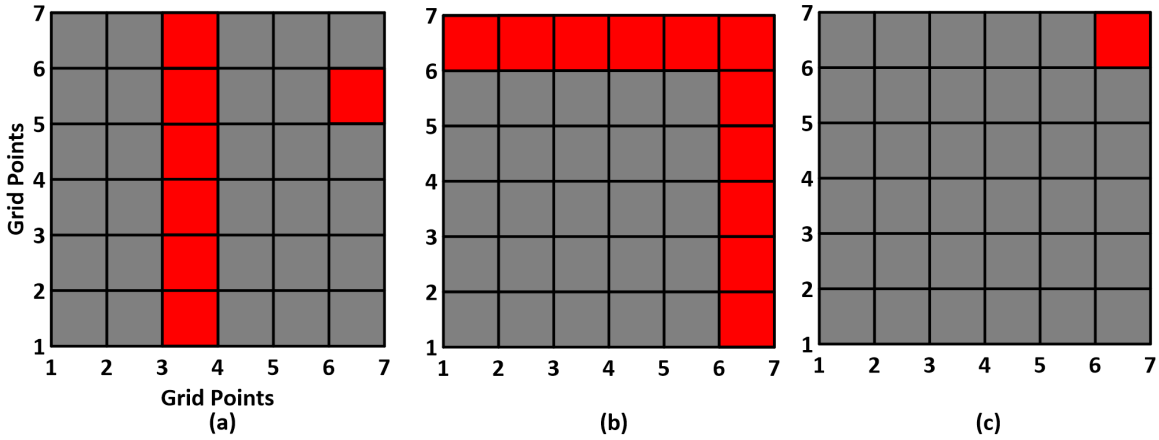

Figure 8. Block diagram representing the resolution matrix values obtained in individual blocks from the inversion at (a) 0 – 4 km depth, (b) 4 – 8 km depth and (c) 8 -12 km depth, respectively. Grey color blocks are well resolved (resolution value > 0.7) while the red blocks are poorly resolved (resolution value < 0.7).

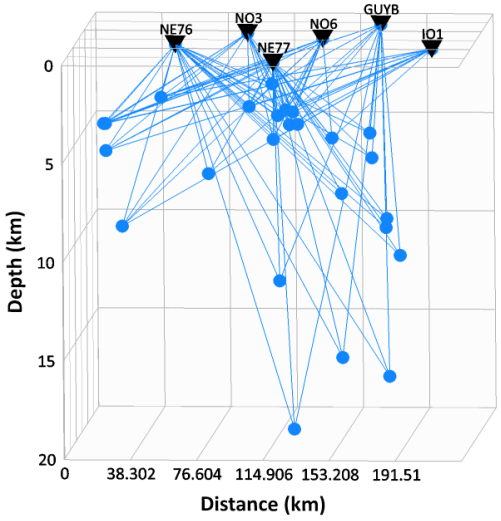

Figure 10. Ray-path diagram illustrating the coverage of different blocks between the events and their respective recording stations. The events are represented by the blue dots and the station shown by the inverted black triangles.

The inversion algorithm gives three-dimensional attenuation structure at 18 different frequencies at which spectral input data has been used. The three-dimensional attenuation structure at 0.5 Hz, 1.0 Hz and 2.0 Hz, respectively, are shown in Fig. 10, 11 and 12. The blocks with low-resolution values have been covered with white blocks.

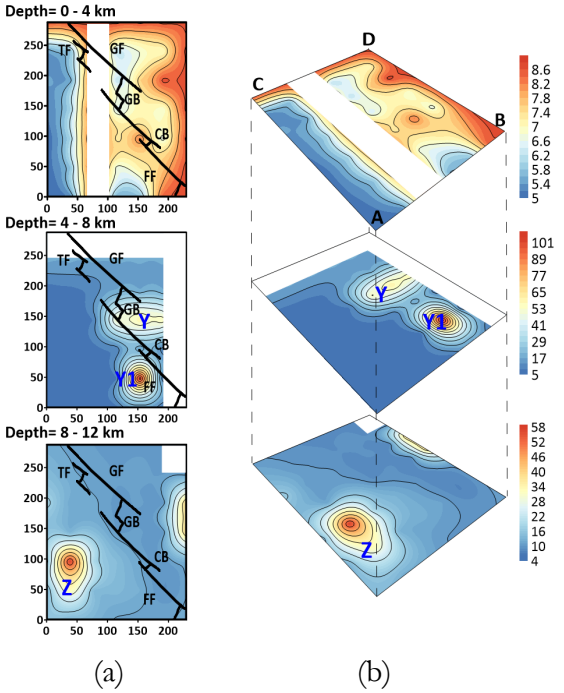

Figure 10. Quality factor contours obtained from the inversion at 0.5 Hz frequency for (i) 0-4 km (ii) 4-8 km (iii) 8-12 km depths. The solid line in (a) represents the tectonic features present in the study region. Labels Y, Y1 and Z represent the high Q patches observed at various depths. Blocks of lower resolution are covered by the white rectangular blocks.

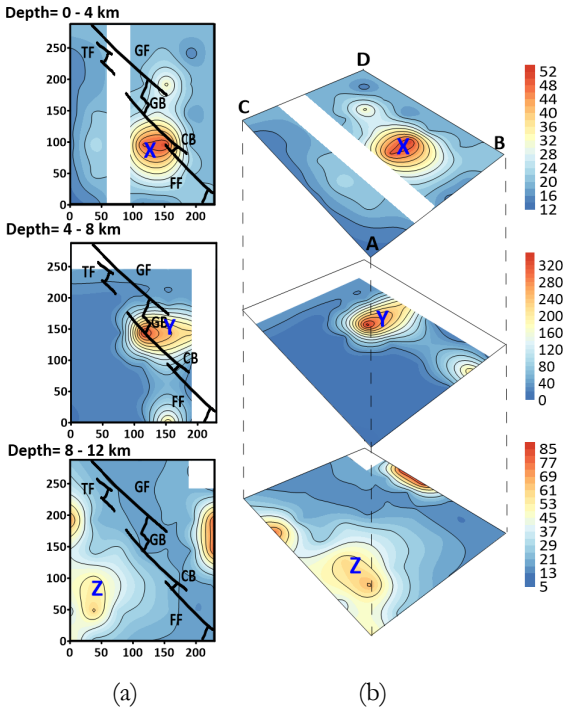

Figure 11. Quality factor contours as in Fig. 9 but at 1.0 Hz for (i) 0-4 km (ii) 4-8 km (iii) 8-12 km depths. The solid black line in Fig. (a) represents the tectonic features present in the study region. Labels X, Y and Z points out high Q patches observed at various depths. Blocks of lower resolution are covered by the white rectangular blocks.

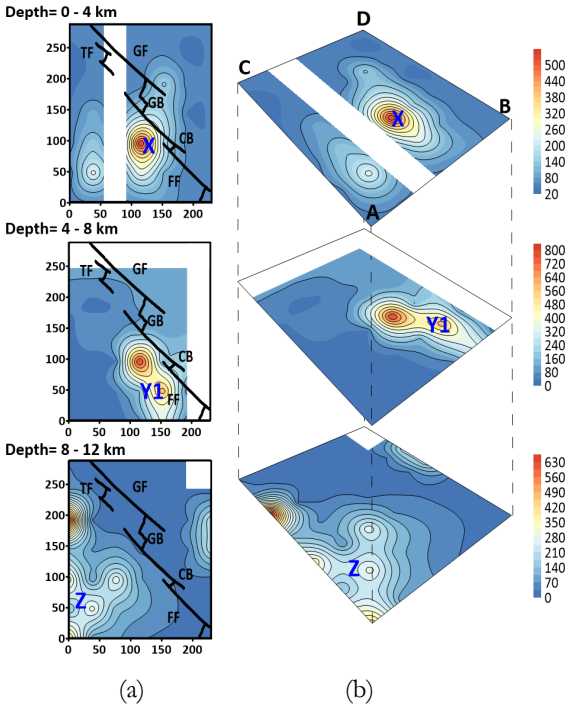

Figure 12. Quality factor contours at 2.0 Hz for (i) 0-4 km (ii) 4-8 km (iii) 8-12 km depths. The solid line in (a) represents the tectonic features present in the study region. Labels X, Y1 and Z points out the high Q patches observed in the studied region at various depths. Blocks of lower resolution are covered by the white rectangular blocks.

The attenuation contours obtained from the inversion are useful for identifying the different patches of low and high Q values at different depth layers. The results obtained shows low Q values along the gulf region, particularly at shallow depths. The attenuation structure obtained is correlated with the crustal velocity structure determined by Lizarralde *et al.,* (2007) and Teske *et al.,* (2014). Fig. 13 summarizes the crustal structure of the Guaymas basin, located in the centre of the studied region of the gulf.

For the surface layer (0-4 km), the low Q values contrast with one major patch (zone X in figures 11 and 12) of high Q value in the south-east zone of the region. The crustal structure obtained by Aragón-Arreola *et al.,* (2005), Lizarralde *et al.,* (2007) indicates that the south-central region of GoC, is masked by a thick layer of sill intruding the sediments deposited on the igneous layer. Thus, resulting in the low Q value and high attenuation in the surface layer. But the thickness of this sediment layer decrease from ~ 3 km in the Guyamas basin to the ~1.5 km in the Carmen basin. Thus, the presence of the igneous layer (Teske *et al.,* (2014)) in the surface layer results in the increase of Q (zone X) in the south-east of the studied region, as shown in Figs. 11-12 at 1.0 Hz and 2.0 Hz. This feature does not show at the lower frequency (0.5 Hz) probably due to the small dimension of the high Q patch.

In the middle layer (4-8 km depth), two major patches (zones Y and Y1) of high Q value can be observed close to the ridge- transform system. First, the high Q patch Y at 0.5 and 1.0 Hz along the Guyamas basin increases with frequency from 53 at 0.5 Hz to 320 and 800 at 1.0 and 2.0 Hz, respectively. The subsurface representation of Guaymas basin shown in Fig. 13 suggest the presence of high heat flow due to intruded sills located along the western side of the spreading ridge. Thus, the cooler southwestern side has a higher Q value compared to the hotter northeastern side of the Guaymas Basin. The other high Q patch Y1 located along the Farallon Transform fault in a zone of high seismicity, where the rocks must be cool and rigid.

In the bottom Layer (8-12 km depth), a high Q value patch (Z) is observed along with the older and cooler continental crust. The obtained Q values in the depth range show a decreasing trend

of Q towards the spreading ridges. This 8-12 km depth zone probably has a high flow of magma from the mantle near the ridge, as shown in Fig. 13, resulting in an increase of thermal flow in the bottom layer. Thus, low Q values and high S-wave attenuation takes place along the ridge transform fault system.

The obtained attenuation contours correlate with the crustal model proposed by Lizarralde *et al.,* (2007) and Teske *et al.,* (2014) and support the high attenuation of seismic energy observed along the gulf region. Also, the decrease in seismic velocity and high heat flow beneath the thin crust correlates with the high attenuation observed along the young plate boundary (Persaud *et al.,* 2014; Teske *et al.,* 2014; Vidales-Basurto *et al.,* 2014; Lizarralde *et al.,* 2007; Hasegawa 1985). These results also indicate that the seismic attenuation is decreasing towards the continental crust.

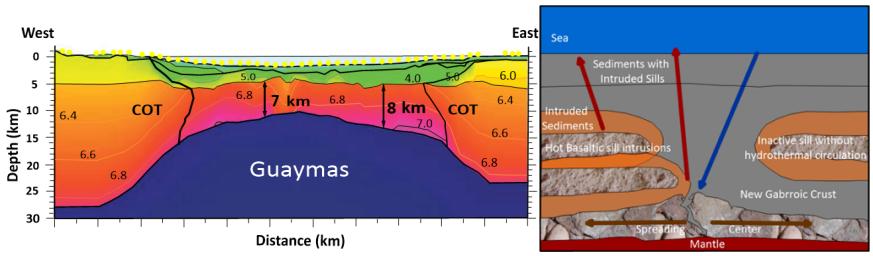

(a) (b)

Figure 13. (a) Seismic velocity and crustal model for Guaymas extensional basin region of GoC, Mexico (modified after Lizarralde *et al.,* 2007). (b) schematic diagram of subsurface basement, sills, sediments and arrow represent the liquid flow direction (modified after Teske *et al.,* 2014).

BOOTSTRAP TEST

In order to inspect the stability of inverted Q structures, the bootstrap resampling scheme has been adopted. For the same, the initial population of 25 earthquakes has been divided into two subsets, with each subset having randomly selected 17 earthquakes. The inversion results for 1.0 Hz frequency are shown in Fig 14.

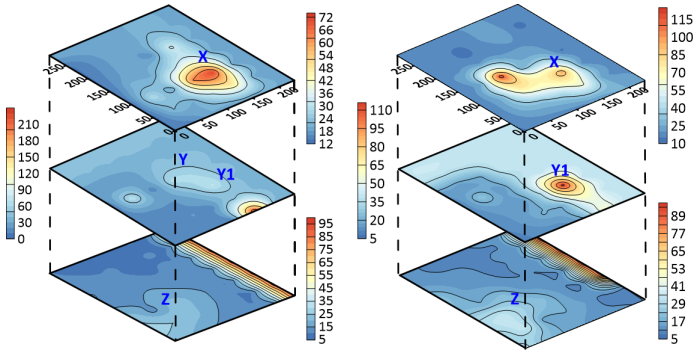

(a) (b)

Figure 14. Bootstrap test results for two different subsets of initial population of earthquakes for depths (i) 0-4 km (ii) 4-8 km and (iii) 8 -12 km at 1 Hz frequency. The alphabets X, Y, Y1 and Z represents the identified low attenuation zones in different depth layers.

The comparison of bootstrap test results with Figs. 10-12, clearly reveal that for different subset of initial population of earthquakes, we are capable of detecting the same attenuation features on different depth layers. Thus, the resulted Q structure in this study is stable and consistent for

different subset of original dataset. However, decreasing the number of earthquakes in bootstrap test has lowered the resolution of individual rectangular blocks, so few major differences in the attenuation structure has been observed in the bootstrap results.

A regional Q-frequency relation for this region has been prepared by using all 1944 estimates of shear wave quality factor at 18 different frequencies. Fig. 15 and 16 show the Q-frequency relation obtained using average values of Q_s resulting from the inversion for each frequency. The best least square fit gives the relation $Q_s(f) = 20f^{1.2}$ for this region. Fig. 15 shows data used for obtaining this relationship. It has been observed that seismic Q strongly depends on the frequency f in the view of relation $Q = Q_0 f^n$ and increases with increase of frequency (Aki, 1980a). But this increase is not so widespread at low frequencies in comparison to high frequencies as we move from surface to depth (Kumar *et al.,* 2015). Therefore, a relatively large error has been measured at high frequencies as shown in Fig. 15. Despite the large variation in Q_s values at high frequencies, the resulted Q_s values are providing the significant information for south-central GoC region.

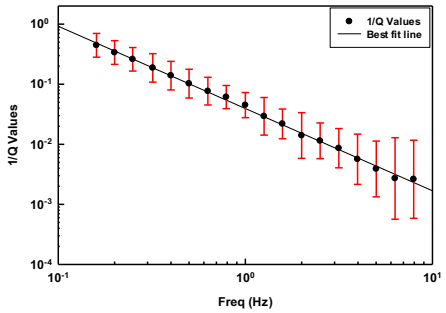

Figure 15. Frequency - dependent shear wave quality factor $1/Q_s(f)$ relationship obtained from 1944 values of shear wave quality factor at different frequencies.

The Q_0-f^n relation can be used to distinguish different regions into seismically active and stable areas. The parameters Q_0 and n represent heterogeneities and levels of tectonic activity, respectively (Kumar *et al.,* 2015). Low values of $Q_0 < 200$ indicate tectonically and seismically active regions, high values of $Q_0 > 600$ signify seismically stable regions, and intermediate values are expected in moderately active regions (Kumar *et al.,* 2005). A correlation between the degree of frequency dependence and the level of tectonic activity in the area of measurement have been made by several researchers for a number of tectonic regions (e.g., Aki, 1980a; & Van Eck, 1988). They ascertained higher n values for tectonically active regions as compared to that of tectonically stable regions (Sharma *et al.,* 2015). The obtained low Q_0 =20 and high exponent n=1.2 of this relation indicate that the studied region is highly active with high attenuation. The resulted high value of n=1.2 is an artifact and can be considered as ~1.0. Similar, higher values of exponent n, has also observed for various highly active regions of world (Gupta *et al.,* 1988, Akinci *et al.,* 1994 & Vidales-Basurto *et al.,* 2014).

We compare in Fig. 16, obtained relation with regional relationships obtained by previous studies in the GoC region using different techniques. It is seen that Q_0-f^n relation obtained with the estimates of Q from the inversion matches with other relations obtained for this region within the variability of the estimates shown in Fig. 15. The higher values of Q reported by Vidales-Basurto *et al.,* (2014) are due to differences in the crustal volume sampled. Most of the paths sampled by them are outside the ridge zone and some includes the continental region. The estimates of Castro *et al.,* (2008) correspond to the Mexican Basin and Range Provence, inside the continent. The estimates of Q from the Imperial

Valley (Singh *et al., 1982)* are very similar to our estimates in south-central Gulf of California. These two regions have some geologic features in common, like the presence of sediments and high heat flow and explain the low values of Q obtained.

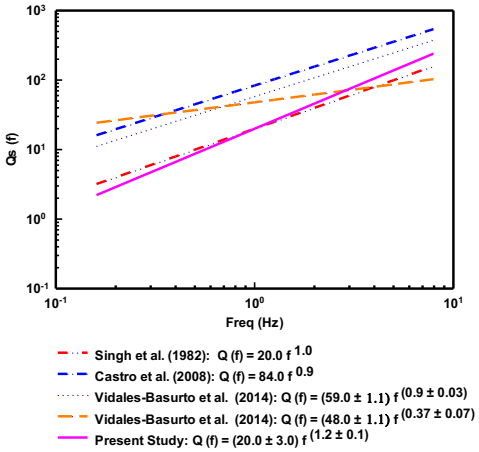

Figure 16. Comparison of obtained Q_0-f^n relation with other existing relations for the south-central GoC region.

CONCLUSIONS

A frequency-dependent three-dimensional shear wave attenuation structure for the south-central Gulf of California, Mexico has been obtained using 98 records from 25 earthquakes recorded at six different stations. A total of shear wave attenuation structures at 18 frequencies has been obtained in this work that permitted us to identify zones of high and low attenuation that correlate well with geological and tectonic models of the region. The iterative inversion scheme used in this work gives results consistent with crustal models proposed by Lizarralde *et al.,* (2007) and Teske *et al.,* (2014) for the Gulf of California region. The average shear wave quality factor obtained from the different 108 blocks at different frequencies from inversion has been further used to develop the regional frequency dependent shear wave quality factor of form $Qs\ (f) = 20\ f^{1.2}$. The developed relationship has been compared with that available for this region. The comparison establishes the reliability of obtained shear wave quality factors in different blocks.

ACKNOWLEDGEMENTS: Authors sincerely thank the Indian Institute of Technology, Roorkee, Roorkee, Uttarakhand, India and Centro de Investigación Científica y de Educación Superior de Ensenada (CICESE), Baja California, Mexico for supporting the study presented in this article. We acknowledge Dr. Claudia Vidales-Basurto and Dr. Lenin Avila-Barrientos, who provided the site response functions used. We thank Antonio Mendoza and Arturo Pérez-Vertti for facilitating data from the RESBAN array. The work presented in this paper is the outcome of the DST project grant no. DST/INT/MEXICO/P-03/2016; CONACYT-DST 266078 and CONACYT CB2017-2018-A1-S-37179. We would also like to thanks Dr. Roberto Ortega, CICESE, Mexico for his efforts and expertise for reviewing the manuscript, to improve the quality of article.

REFERENCES:

Aki, K. & Lee, W.H.K. (1976). Determination of the three- dimensional velocity anomalies under a seismic array using first p arrival time from local earthquakes. 1. A homogeneous initial model. *Journal of Geophysical Research, 81,* 4381-4399.

Aki, K., & Chouet, B. (1975). Origin of coda waves: source, Attenuation and scattering effects. *Journal of Geophysical Research, 80,* 3322-3342.

Akinchi, A., Taktak, A. G., and Ergintav, S. (1994). Attenuation of coda waves in western Anatolia. *Physics of Earth and Planetary Interiors,*87, 155–165.

Aki, K, (1980a). Attenuation of shear waves in the lithosphere for frequencies from 0.05 to 25 Hz. *Physics of Earth and Planetary Interiors, 21,* 50-60.

Aragon-Arreola, M. & Morandi, M. (2005). *Structure of the rift basins in the central Gulf of California; kinematic implications for oblique rifting. Tectonophysics, 409,* 19-38.

Avila-Barrientos, L. & Castro, R.R. (2016). Site response of the broad band stations of the NARS-Baja and RESBAN arrays, located in the region of the Gulf of California, México. *Geofísica Internacional,* 55, 131-154.

Backus, G.E., & Gilbert, J.F. (1968). The resolving power of gross earth data. *Geophysical Journal International, 16*, 169-205.

Bennett, S., Oskin, M., & Iriondo, A. (2007). Transition from Proto-Gulf extension to transtension, coastal Sonora, Mexico. *Eos, Trans. American Geophysical Union, 88*, 23.

Besana, G.M., Negishi, H. & Ando, M. (1997). The three-dimensional attenuation structures beneath the Philippine archipelago based on seismic intensity data inversion. *Earth and Planetary Science Letters, 151*, (1997).

Castro, R., Condori, C., Romero, O., Jacques, C., & Suter, M. (2008). Seismic Attenuation in Northeastern Sonora, Mexico. *Bulletin of the Seismological Society of America, 98(2),* 722-732.

Castro, R.R., Pérez-Vertti, A., Mendez, I., Mendoza, A., & Inzunza, L. (2011b). Location of moderate size earthquakes recorded by the NARS-Baja array in the Gulf of California region between 2002 and 2006. *Pure & Applied Geophysics, 168,* 1279–1292.

Castro, R.R., Stock J.M., Hauksson E., and Clayton R.W. (2017a). Source functions and path effects from earthquakes in the Farallon Transform Fault region, Gulf of California, Mexico that occurred on October 2013, *Pure and Applied Geophy*sics, 174 (6), 2239-2256.

Castro, R.R., Stock, J.M., Hauksson, E. & Clayton, R.W. (2017b). Active tectonics in the Gulf of California and seismicity (M > 3.0) for the period 2002– 2014. *Tectonophysics, 719–720,* 4–16.

Castro, R.R., Mendoza-Camberos, A. & Perez-Vertti A. (2018a). The broadband seismological network (RESBAN) of the Gulf of California, Mexico, Seismological Research Letter, 89.

Castro R.R., Mendoza-Camberos, A. & Pérez-Vertti A. (2018b). Radiated seismic energy of earthquakes in the south–central region of the Gulf of California, Mexico. *Geophysical Journal International, 214 (2),* 990-1003.

Castro, R. R., Singh, S. K., Joshi, A., and Singh, S. (2019). Shear wave attenuation study in the south region of the Gulf of California, Mexico. *Bulletin of Seismological Society of America, 109,* 600–609.

Dorsey, J.R., Umhoefer, J.P., Oskin, E.M. & Arrowsmith, R. (2013). Rupturing Continental Lithosphere in the Gulf of California & Salton Trough. *GeoPRISMS Newsletter, Issue No. 30.*

Goff, J.A., Bergman, E.A., Solomon & S.C. (1987). Earthquake source mechanism and transform fault tectonics in the Gulf of California. *Journal of Geophysical Research*, 92, 10, 485–10, 510.

Gupta, S. C., Teotia, S. S., Rai, S. S., and Gautam, N. (1998). Coda Q estimates in the Koyna region, India. *Pure and Applied Geophysics, 153,* 713–731.

Hashida, T. & Shimazaki, K. (1984). Determination of seismic attenuation structure and source strength by inversion of seismic intensity data: method and numerical experiment. *Journal of physics of Earth, 32*, 299-316.

Hasegawa, H.S. (1985). Attenuation of Lg waves in the Canadian Shield. *Bulletin of the Seismological Society of America,75,* 1569 – 1582.

Joshi, A. (2007). *Inversion of seismic intensity data for the determination of three-dimensional attenuation structures in the central gap region of Himalayas. Natural Hazards 43*, 129–146.

Joshi, A., Mohanty, M., Bansal, A.R., Dimri, V.P., & Chadha, R.K. (2010). Use of spectral acceleration data for determination of three- dimensional attenuation structure in Pithoragarh region of Kumaon Himalayas. *Journal of Seismology, 14,* 247–272.

Knopoff, L. (1964). Q. *Reviews of Geophysics, 2*, 625-660.

Kumar, N., Parvez, I.A. & Virk, H.S. (2005). Estimation of coda wave attenuation for NW Himalaya region using local earthquakes. *Physics of Earth and Planetary Interiors, 151,* 243-258.

Kumar P., Joshi A., Sandeep, Kumar A., & Chadha R.K. (2015). Detailed attenuation study of shear waves in the Kumaon Himalaya, India, using the inversion of strong-motion data. *Bulletin of the Seismological Society of America, 105(4)*, 1836–1851.

Lonsdale P., (1989). Geology and tectonic history of the Gulf of California, in Winterer, E.L., *et al*., eds., The Eastern Pacific Ocean and Hawaii:Boulder, Colorado, *Geological Society of America, Geology of North America, v. N, p.499–521.*

Luccio F. Di, Persaud P., & Clayton R.W. (2014). Seismic structure beneath the Gulf of California: a contribution from group velocity measurements. *Geophysical Journal International, 199,* 1861–1877.

Lizarralde, D., Axen G.J., Brown H.E., Fletcher J.M., González-Fernández A., Harding A.J., Holbrook W.S., Kent G.M., Paramo P., & Sutherland F. (2007). Variation in styles of rifting in the Gulf of California. *Nature, 448,* 466 – 469.

Nakamura, R. & Uetake, T. (2002): Three-dimensional attenuation structure and site amplification inversion by using a large quantity of seismic strong motion records in Japan. *Journal of the Seismological Society of Japan, 54,* 475-488.

Ortega, R., and González, M. (2007). Seismic wave attenuation and source excitation in La Paz-Los Cabos, Baja California Sur, Mexico. *Bulletin of Seismological Society of America, 97,* 545–556.

Ortega, R., and Quintanar, L. (2010). Seismic evidence of a ridge-parallel strike-slip fault off the transform system in the Gulf of California. *Geophysical Research latter, 37,* L06301.

Ortega, R., and Quintanar, L. (2011). A comparison between P-wave and S-wave propagation characteristics in the southern part of the Gulf of California, Mexico. *Bulletin of Seismological Society of America, 101,* 1270– 1280.

Pacheco, J.F. & Sykes L.R. (1992). Seismic moment catalog of large shallow earthquakes,1900 to 1989. *Bulletin of the Seismological Society of America, 82,* 1306–1349.

Paulssen, H., & de Vos, D. (2017). Slab remnants beneath the Baja California peninsula: seismic constraints and tectonic implications. *Tectonophysics, 719–720,* 27–36.

Persuad, P., Stock J.M., Steckler, M.S., Martin-Barajas, A., Diebold, J.B., Gonzalez-Fernandez, A. & Mountain, G.S. (2003). Active deformation and shallow structure of the Wagner, Consag, and Delfin basins, northern Gulf of California, Mexico. *Journal of Geophysical Research, 42(6),* 2355.

Persaud P., Luccio, F.Di., & Clayton R.W. (2014). Rayleigh wave dispersion measurements reveal low-velocity zones beneath the new crust in the Gulf of California. *Geophysical Research Letters, 42(6),* 1766-1774.

Quintanar, L., Ortega, R., Rodríguez-Lozoya, H.E., Domínguez-Reyes, T. (2019). The 4 January 2006 (M w 6.6), San Pedro Martir Earthquake: Example of an Earthquake for Calibrating Excitation and Attenuation Studies. *Bulletin of the Seismological Society of America, 109(6),* 2399–2414.

Rebollar, C.J., Quintanar, L., Castro, R.R., Day, S.M., Madrid, J., Brune, J.N., Astiz, L. & Vernon, F. (2001). Source characteristics of a 5.5 magnitude earthquake that occurred in the transform fault system of the Delfin Basin in the Gulf of California. *Bulletin of the Seismological Society of America, 91*, 781–791.

Rodríguez-Lozoya, H.E., Domínguez R.T., Quintanar R.L., Meléndez A.A., Rodríguez-Leyva H.E., Rocha W.P. & García-Páez F. (2017). Attenuation of Coda Waves in the Central Region of the Gulf of California, México. *Geofísica Internacional 56 (2),* 137-145.

Satake, K. & Hashida, T. (1989). Three-dimensional attenuation structure beneath North Island, New Zealand. *Tectonophysics 159,* 181–194.

Sharma, B., Teotia, S.S. & Kumar, D. (2007). Attenuation of P, S, and coda waves in Koyna region, India. *Journal of Seismology, 11,* 327–334.

Singh S.K., Aspel R.J., Fried J., & Brune J.N. (1982). Spectral attenuation of SH waves along the imperial fault. *Bulletin of Seismological Society of America*, 72, 2003-2016.

Stock, J.M., & Hodges K.V. (1989). Pre-Pliocene extension around the Gulf of California and the transfer of Baja California to the Pacific plate. *Tectonics, 8*, 99–115.

Sumy, D.F., Gaherty, J.B., Kim, W.Y., Diehl, T., & Collins, J.A. (2013). The mechanism of earthquakes and faulting in the southern Gulf of California. *Bulletin of the Seismological Society of America, 103,* 487–506.

Teske, A., Callaghan A.V., & LaRowe D.E. (2014). Biosphere frontiers of subsurface life in the sedimented hydrothermal system of Guaymas Basin. *Frontiers in Microbiology* 5:362.

Trampert, J., H. Paulsen, A. Van Wettum, J. Ritsema, R. Clayton, R. Castro, C. Rebollar & A. Pérez-Vertti (2003). New array monitors seismic activity near the Gulf of California in México. *EOS, Trans. American Geophysical Union, 84,* 29-32.

Umhoefer, P.J. (2011). Why did the Southern Gulf of California rupture so rapidly? Oblique divergence across hot, weak lithosphere along a tectonically active margin. *Geological Society of America Today, 21*, 4-10.

Van Eck T. (1988). Attenuation of coda waves in the Dead Sea region. *Bulletin of the Seismological Society of America, 78,* 770–779.

Vidales-Basurto, C.A., Castro, R.R., Huerta, C.I., Sumy, D.F., Gaherty, J.B. & Collins, J.A. (2014). An attenuation study of body waves in the south–central region of the Gulf of California, Mexico. *Bulletin of the Seismological Society of America, 104,* 2027–2042.